
The Dosimetry of Iodine-123-Labeled TISCH: A SPECT Imaging Agent for the D1 Dopamine Receptor

P. David Mozley, Xiaowei Zhu, Hank F. Kung, Mark H. Selikson, James Hickey, Suzanne Galloway, Nula Pfeiffer and Abass Alavi

Division of Nuclear Medicine, Department of Radiology, University of Pennsylvania, Philadelphia, Pennsylvania

TISCH is an iodinated D1 specific dopamine receptor antagonist that may be useful as a SPECT imaging agent. This report documents its pharmacological safety in animals and its radiation dosimetry in humans. The dose of radiation that ^{123}I -TISCH delivered to seven healthy subjects was estimated with the absorbed fraction technique. Conjugate images of the body were serially acquired for up to 24 hr after the administration of a known amount of activity. The count rates in the organs that could be visualized were measured on each image. These count rates were corrected for attenuation with ^{123}I transmission scans. The doses to the other organs that did not take up enough activity to be visualized on the images were estimated with established models. The dosimetry was calculated for each subject individually before the results were averaged. Rapid biological washout minimizes the radiation exposure to most organs. The dose to the large bowel is limiting in healthy volunteers. The proximal colon receives about 0.67 rad/mCi (180 $\mu\text{Gy}/\text{MBq}$) or about 5 rads for every 7.5 mCi of TISCH injected. This low radiation burden should make it feasible to study the D1 dopamine receptor in patients who have neuropsychiatric disorders before and after treatment.

J Nucl Med 1993; 34:208-213

Neuroimaging studies of the D1 dopamine (DA) receptor may further the understanding of normal brain function and the pathophysiological basis of several neuropsychiatric disorders. The distribution of this receptor in regions of the neocortex, such as the dorsolateral prefrontal cortex, the hippocampus and the amygdala, suggests that it may play an intimate role in several cognitive functions (1). Decreased D1 DA activity may be associated with some of the cognitive deficits that characterize schizophrenia (2,3), since intellectual performance seems to improve in some of these patients with the administration of a D1 specific agonist (4). Decreased D1 DA activity may also contribute to the formation of psychotic symptoms. The

positive symptoms of psychosis are thought to result from processes that increase the activity of D2 dopaminergic neurons (5). Animal studies have demonstrated that the D1 dopaminergic neurons in the cortex tend to inhibit D2 activity in the mesolimbic system (6,7). Decreased D1 inhibition of these D2 neurons may result in pathologically increased D2 activity that produces some of the positive symptoms of psychosis. Unfortunately, these relationships have been difficult to study in living patients, in part because a D1 specific dopamine receptor ligand that can be used with conventional neuroimaging techniques has not become widely available.

Several Schering compounds are highly specific D1 receptor antagonists. They have been useful in laboratory studies of animals and in postmortem specimens (8). Schering compounds 23390 and 39166 have been labeled with ^{11}C for use with positron emission tomography (9,10), but they have not been satisfactorily labeled with a radionuclide that can be used in vivo with single-photon emission computed tomography (SPECT).

Kung and his colleagues (11-13) have developed a series of iodinated Schering compounds which include the 3-iodo analog of 23390, referred to as TISCH [(+)-7-chloro-8-hydroxyl-1-(3'-iodophenyl) 3-methyl-2,3,4,5-tetrahydro-1H-3-benzazepine]. TISCH has a K_d of 0.03 nM in striatal membrane preparations derived from rats (13). Its binding can be blocked by D1 specific Schering compounds (13) and reduced by both direct and indirect DA agonists (14). Because its relative uptake in the brains of animals is high with a favorable target-to-background ratio (15), studies were done of its pharmacological safety in animals and its dosimetry in humans.

METHODS

Toxicology Studies

Nonradioactive TISCH was administered intravenously to seven male New Zealand White rabbits in doses of 82.6 mg/kg/day (0.7 mmol/kg/day) 5 days a week for 2 wk. Seven matched control rabbits were injected with placebo. Serial measurements were made of their weights, basal body temperatures and serum chemistries. Both groups were monitored for 2 wk after treatment before they were killed. Histopathological examinations that fol-

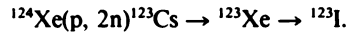
Received Dec. 3, 1991; revision accepted Sept. 2, 1992.

For correspondence or reprints contact: P. David Mozley, MD, Division of Nuclear Medicine, 110 Donner Building, H.U.P., 3400 Spruce St., Philadelphia, PA 19104.

lowed included gross and microscopic inspections of the brain, kidneys, liver, lungs and testes.

Radionuclide

The ^{123}I used in this study was obtained commercially (Nordion Intl., Canada). It was generated with the reaction



This cyclotron-based production scheme does not produce any ^{124}I or ^{125}I contamination. The radionuclide purity of each dose was guaranteed to exceed 99.8%.

Radiolabeling

The preparation of the radiotracer labeling kit has already been described in detail (13). This kit contained 50 μg of the lyophilized tributyl tin derivative, $\text{SnBu}_3\text{-TISCH}$. After adding about 12 mCi of ^{123}I NaI dissolved in a 50% solution of ethanol and hydrochloric acid, an iododestannylation reaction was initiated with hydrogen peroxide and quenched with sodium bisulfite. After purging the volatile side products with air, the reaction mixture was neutralized with sodium bicarbonate and extracted with ethyl acetate. The radiolabeled TISCH was separated from any impurities with preparative reverse-phase, high-pressure liquid chromatography (HPLC). The fraction corresponding to the ^{123}I -TISCH was collected and condensed before being dissolved in ethanol and diluted with 2.0 ml of normal saline. This solution was passed through a 0.22 μm filter prior to administration.

A small volume of the final solution was removed and analyzed for purity with HPLC. Another aliquot was retained for sterility and pyrogenicity tests.

Accrual and Assessment of Subjects

Seven men with a mean age of 31 ± 6.8 (range: 23–41) gave informed consent. A structured medical history and physical examination indicated that they were healthy and without any disease processes that could potentially effect the distribution or elimination of the radioligand in a meaningful way. Each took ten drops of Lugol's solution prior to the study, which was administered after the initial laboratory studies had been drawn.

Blood was drawn an hour before and 24 hr after administration of the tracer. The clinical laboratory battery included a complete blood cell count with differential, serum electrolytes, liver enzymes, thyroid function tests, an autoimmune panel, urinalysis and a urine drug screen.

Measurements of Linear Attenuation

Each subject was positioned between a sheet source and a gamma camera so that their mid-coronal panel was 35 cm from the surface of a parallel hole collimator. The sheet source contained between 4 and 8 mCi of ^{123}I in 500 ml of water. Transmission images were acquired for 2 min through air and each organ. The fraction of attenuated activity was determined by dividing the transmitted counts per pixel through an organ by the counts per pixel in an unattenuated image of the sheet source.

Measurements of Administered Activity

The amount of radioactivity in each syringe containing ^{123}I -labeled TISCH was measured in a Radcal 4045 dose calibrator before and after injection. The doses that were administered in this study ranged from 1.8 to 3.1 mCi. Images of these syringes were also acquired before and after injection on the same gamma camera that was used to scan the subjects. Images of the injection sites were checked to make sure that the doses had not infiltrated the subcutaneous tissue.

Emission Images

Conjugate images were obtained for 2 min each on a single-headed SPECT system (GE Medical Systems, Milwaukee, WI). It was equipped with a large field of view, low-energy, all-purpose, parallel-hole collimator. A 20% window was symmetrically centered on 159 keV. The dose was administered at about 4 p.m. (1600 hr). The first set of images was acquired about 1 hr later. Between four and six sets of images were obtained over the next 9 hr. Another set of images was acquired the next day in five of the seven subjects.

Count Rate Measurements

Two methods were used to measure the count rates in organs that took up enough activity to be visualized on the images. The clearest image of each organ was displayed on a gray scale, with the upper limit automatically set for the pixel of maximum intensity. The operator then subtracted 10% as background. An automated subroutine counted the number of pixels in a region of interest (ROI) that was made by tracing the edges of the organ with a tract ball. A subset of 54 ROIs was drawn twice in order to quantify the intra-rater reliability of these measurements.

The rapid elimination of this SPECT agent obscured the boundaries of most organs on the delayed images. Whenever the boundaries of an organ could not be clearly visualized, the total number of counts in its image was calculated by first placing a limited ROI within the organ and measuring the mean counts per pixel in the ROI. With the exception of the right lung base, these ROIs were made as large as possible, while ensuring that they fell completely within the organ borders. The average counts per pixel in these ROIs was then multiplied by the total area of the organ that was measured on its clearest image.

A subset of 17 organs was measured both ways on their initial images in order to quantify the effect of using a limited boundary instead of a whole organ boundary.

Quantitation of Activity

A version of the absorbed fraction technique was used to quantify the fraction of the injected activity C_i , in each organ at each time point (16–19). These fractions were calculated from the count rates that were measured on the images with the equation:

$$C_i(t) = \frac{\sqrt{\frac{C_a(t) \times C_p(t)}{e^{-\mu x}}}}{C_s}, \quad \text{Eq. 1}$$

where $C_i(t)$ = fraction of the administered dose at time t ;

$C_a(t)$ = anterior view count rate at time t (cpm);

$C_p(t)$ = posterior view count rate at time t (cpm);

μ = effective linear attenuation coefficient (cm^{-1});

x = effective thickness of the patient over the organ of interest (cm);

C_s = difference in the syringe count rates pre- and postinjection (cpm).

The value of $[e^{-\mu x}]$ was measured directly from the transmission images. The correction factor for organ geometry that is usually included in Equation 1 was assumed to be unity.

Cumulated Activity

The cumulated activity, \tilde{A}_i , within an organ depends on how much of the radiotracer it takes up and how long the activity resides in the organ. In this study, curve fitting was not neces-

sary to integrate the time-activity curves because the cumulated activity in an organ could be calculated directly with Equation 2 below:

$$\tilde{A}_i = A_1 t_1 + \sum_{j=1}^{n-1} 1/2[A_i(t_j) + A_i(t_{j+1})][t_{j+1} - t_j] + \frac{A_n(t_n)}{\lambda_p}, \quad \text{Eq. 2}$$

where \tilde{A}_i is the cumulated activity in the i^{th} organ ($\mu\text{Ci-hr}$), A_1 is the activity in the i^{th} organ at the first time point (μCi), A_i is the measured activity in the i^{th} organ (μCi), t_1 is the time interval between injection and the first set of emission images (hr), t_j is the time interval between injection and the j^{th} set of emission images (hr) and n is the total number of images made over the course of the study.

The first two terms in the equation represent the summation of areas under the actual time (hours) activity (μCi) curve for each organ. The last term represents the maximum dose an organ could have absorbed after the last measurement of activity was made even if there was no further biological washout, and physical decay was the only means of elimination from that point on.

Bladder Model

Each subject was asked to micturate frequently, but the voiding interval used in the calculations was 3.5 hr. The voided urine specimens were imaged the same way the syringes and the subjects were. The counts in these images were used to determine the fraction of the injected dose excreted by the renal system as a function of time.

The absorbed dose to the bladder was calculated with the method recommended by ICRP 53 (20). In this model, the bladder dose is a function of the total activity in the body, the fraction of the total body activity that is excreted by the kidneys, the renal excretion rate, and the voiding interval. In a one-compartment model, the rate $U(t)$ at which activity will be excreted into the bladder is given by Equation 3:

$$U(t) = fA_T \lambda_b e^{-(\lambda_b + \lambda_p)t}, \quad \text{Eq. 3}$$

where $U(t)$ is the rate at which activity is excreted into the bladder ($\mu\text{Ci/hr}$), f is the fraction of activity which is eliminated by the renal system, A_T is the total amount of activity injected into the body (μCi), λ_b is the biological elimination constant (hr^{-1}) and λ_p is the radioactive decay constant (hr^{-1}).

Assuming the bladder is empty at $t = 0$, then the total activity A_B excreted into the bladder at time (t) can be calculated by integrating Equation 3 to yield:

$$A_B[\mu\text{Ci}] = fA_T e^{-\lambda_p t} [1 - e^{-\lambda_b t}], \quad \text{Eq. 4}$$

This function was fit to the urine collection data in order to determine the fraction of activity which was eliminated by the renal system, f , and the biological elimination constant, λ_b . For a series of regular voiding intervals T_v , the total cumulated activity \tilde{A}_B contained in the bladder is given by Equation 5:

$$\tilde{A}_B[\mu\text{Ci-hr}] = fA_T \left[\left(\frac{1 - e^{-\lambda_p T_v}}{\lambda_p} \right) - \left(\frac{1 - e^{-(\lambda_p + \lambda_b) T_v}}{\lambda_p + \lambda_b} \right) \right] \left[\frac{1}{1 - e^{-(\lambda_p + \lambda_b) T_v}} \right] \quad \text{Eq. 5}$$

Gastrointestinal Model

The model for the gastrointestinal (GI) tract was taken from ICRP 30 (21). The standard mass of tissue in each region of the gut was taken from ICRP 23 (22). The dose to each region of the GI tract was calculated from the count rates in a single ROI that included the entire extrahepatic abdomen. Because the kidneys and the spleen never accumulated enough activity to be visualized on any of the images, they could not be excluded from this ROI. The right upper quadrant boundary of this ROI was drawn along the superior margin of the right colon and the inferior margin of the liver. In patients with high hepatic flexures, this resulted in the inclusion of some liver tissue in the ROI. The left upper quadrant boundary of this ROI was drawn along the base of the heart and the left lung. Its inferior border included most of the pelvis with the exception of the urinary bladder.

Indirect Measurement of Activity in the Rest of the Body

The dose to many organs could not be measured directly because there was never enough uptake in them to be visualized on the images. Any activity not in the organs that could be visualized on the images was assumed to be evenly distributed in the rest of the body. Because there was no way to determine whether or not the retention of the tracer was prolonged in some of these tissues, the biological half-life of elimination in them was assumed to be 24 hr. This activity was calculated with Equation 6:

$$A_{RB}(t_1) = A_T - \sum_{i=1}^m A_i(t_1), \quad \text{Eq. 6}$$

where A_{RB} is the total activity in the rest of the body at $t = 1$, A_T is the total amount of activity that was injected, A_i is the amount of activity in each organ measured at the time of the first scan and m is the number of organs that were measurable on the images.

Absorbed Doses

The absorbed doses were estimated according to the MIRD formalism (23). The dose to the ovaries was calculated by assuming that a female would have the same percent uptake per somatic organ and whole body as the men in this study.

The equation that was used to calculate the dose D of radiation absorbed by each organ is given by (24):

$$D_k[\text{rad}] = \sum_{i=1}^n \tilde{A}_i S(k \leftarrow i), \quad \text{Eq. 7}$$

where D_k is the dose to target organ k [rad], \tilde{A}_i is the cumulated activity in source organ i ($\mu\text{Ci-hr}$) and $S(k \leftarrow i)$ is the mean dose to target organ k per unit of cumulated activity in source organ i ($\text{rad}/\mu\text{Ci-hr}$).

RESULTS

None of the rabbits who were administered large doses of TISCH for 10 days had any behavioral signs of acute toxicity. When compared to the seven matched control rabbits, their weights and temperatures were stable and they did not develop any meaningful changes in their serum chemistries. Histopathological examinations did not demonstrate any gross or microscopic changes in any of the organ systems that were examined.

HPLC demonstrated that the minimum radiochemical

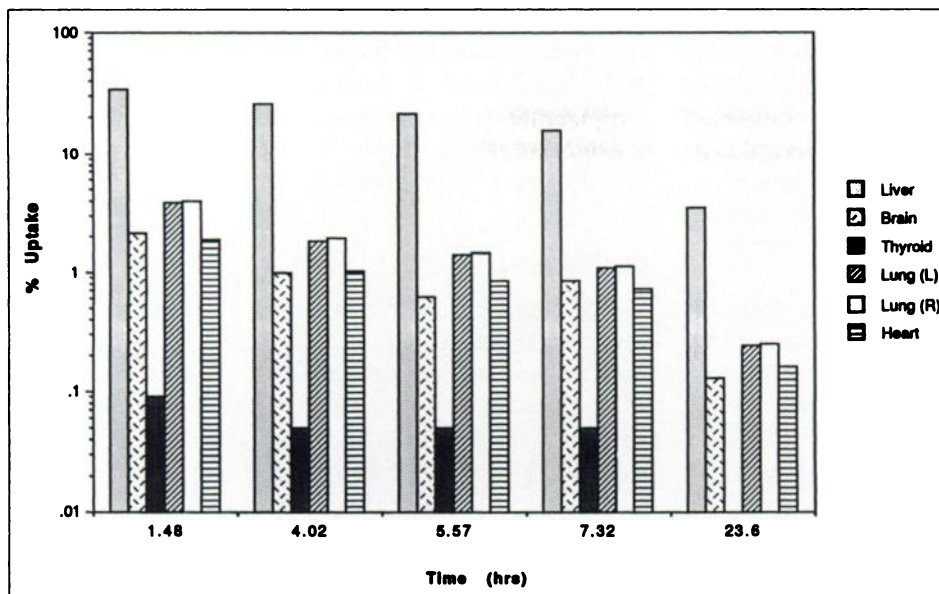


FIGURE 1. The percent uptake over time for the target organs of one subject. The histogram represents the fraction of activity in each organ that was measured over 24 hr.

purity of ^{123}I -TISCH used in this study was $\geq 95\%$. The preparation never failed any other tests of quality control. Pyrogenicity tests were all negative.

The neuroligand was successfully administered to each subject. Images of the injection sites did not show any infiltrated activity. No free activity could be visualized in the salivary glands or stomach. The doses used in this study ranged from 1.8 to 3.1 mCi. The measured count rates in the images of the syringes ranged from 210 to 440 thousand counts per minute. There was no evidence to suggest that these count rates ever approached the saturation rate of the camera. The images were acquired without any untoward events. No artifacts were introduced.

There were no subjective effects of the radiotracer on

any of the subjects. Their vital signs remained stable throughout the procedure, and there were no changes noted on physical examination. There were no meaningful changes in the blood counts or serum chemistry values in any of the subjects.

Analysis of the urine data showed that six of the subjects voided over half the administered activity within the first 8 hr of administration. Rapid clearance of this tracer prevented the boundaries of many organs from being clearly seen on the delayed images.

In a sample of 54 organs with well-delineated boundaries on the early images, ROIs could be drawn around a whole organ with an intra-rater reliability of 94%. However, the measurements of organ area on the delayed images some-

TABLE 1
Organ Dosimetry*

Organ	Dose (mrad/mCi)	\pm s.d. [†] (mrad/mCi)	Dose ($\mu\text{Gy}/\text{MBq}$)	\pm s.d. [†] ($\mu\text{Gy}/\text{MBq}$)	\bar{A} ($\mu\text{Ci}\cdot\text{hr}$)
Bladder wall	210	46	57	12	600
Bone Marrow [‡]	60	5	16	1	
Brain	18	4	5	1	150
Colon: Distal	670	100	180	28	2000
Colon: Proximal	660	100	180	28	2700
Heart wall	80	15	22	4	170
Intestine, Small	270	42	73	11	1200
Kidneys [‡]	50	4	14	1	
Liver	340	41	92	11	4000
Lungs	70	14	19	4	770
Ovaries [‡]	150	17	41	5	
Spleen [‡]	31	3	8	1	
Stomach [‡]	110	17	30	4	370
Testes [‡]	18	3	5	1	
Thyroid	50	16	14	4	9.4
Remainder of the body	50	7	14	2	2200

* All values are the sum of the self dose and the dose from the source organs, which have been rounded to two significant figures.

[†] s.d. = standard deviation. It was calculated in order to indicate the range of values.

[‡] Dose was estimated indirectly from measurements of activity in nearby source organs.

times varied by more than 20%. This problem was dealt with by multiplying the mean activity per pixel in the center of an organ on the delayed images by the total number of pixels in the ROI around the earliest image of it. The effect of this technique was quantified on the early images of 17 organs. It resulted in an overestimation of the total counts by an average of 4.7% when compared to values obtained from the measurements that were made with the whole organ boundary.

These measurements were used to calculate the dosimetry for each subject individually before the results were averaged. The biodistribution of activity over time is shown for one subject in Figure 1. The average dose of radiation received by each organ is listed in Table 1. Visual inspection of the images shown in Figure 2 seems to validate the assumptions and corroborate the calculated results.

TISCH is excreted primarily by the renal system. The

highest concentration of activity occurs within the liver. However, because the transit time through the bowel is much longer than the residence times in the kidney and the liver, the target organ that will limit the amount of activity that can be administered is the proximal colon. It receives about 0.67 rad/mCi (180 μ Gy/MBq).

DISCUSSION

TISCH appears to be a safe SPECT agent. No signs of pharmacological toxicity could be found in rabbits who were administered doses of TISCH which were three orders of magnitude greater than the 20–200 pmole doses that were used in this human study. These doses did not produce any subjective or objective pharmacological effects in the volunteers. The lack of an effect is consistent with a substantial body of medical experience, which sug-

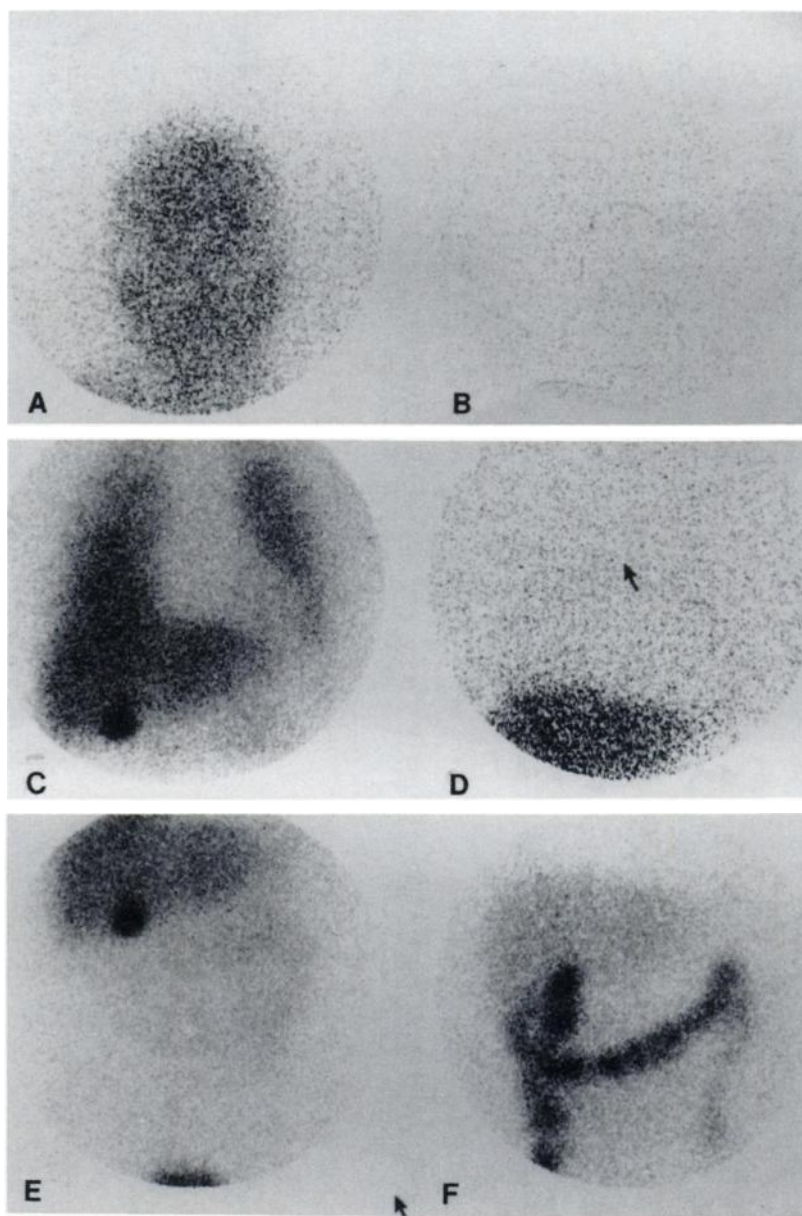


FIGURE 2. Emission images from a 32-yr-old male after the administration of 1.7 mCi of ^{123}I -TISCH. Each picture was acquired for 2 min in the anterior projection. The images on the left were taken about 90 min after injection. The images on the right were taken 24 hr later. (A, B) The head and neck. (C, D) Anterior chest and upper abdomen. The hot spot along the inferior margin of the liver at the bottom of the image on the left is activity in the gallbladder. (E, F) The lower abdomen. Activity in the bladder can be seen in the most inferior aspect of the 90-min image. No activity can be seen in the large bowel on the early images, but the colon becomes increasingly well visualized on the delayed images.

gests that pharmacological doses of dopaminergic drugs in this range do not have a perceptible effect on humans (25).

The MIRD formalism was adapted to the resources that were available for the study. The protocol used to acquire the images resulted in an overestimation of the radiation dose to most organs. The relatively large energy window of 20% centered on 159 keV permitted scattered radiation to contribute to the count rates and increase the apparent radiation burden. However, the increased sensitivity that resulted increased the precision with which an operator could demarcate the organ boundaries on the delayed images.

Placement of small ROIs on the delayed images of most organs also inflated the measurement of the total counts in them. This occurred because these small ROIs were placed in the center of each organ over its region of maximum intensity. The mean activity per pixel in this central ROI was multiplied by the total number of pixels in the ROI enclosing the whole organ on its earliest image, even though the peripheral aspect of most organs contained significantly less activity than the central region. This effect decreased as the relative size of the ROI increased. Because the edges of most organs became progressively more obscure as time passed due to the elimination of the tracer, the size of the ROI tended to become smaller and smaller on the delayed images.

Placement of small ROIs on the transmission scans also increased the dosimetry estimates. The effective linear attenuation for a whole organ was determined from a measurement that was made in its center where it tended to be the thickest.

The method used to calculate the dose to the source organs accounted for any delayed uptake of recirculating activity that had been washed out of another organ up until the time the last image was taken. After the last image was obtained, the effective half-life of elimination in the source organs was assumed to result exclusively from physical decay, as if there was no further biological wash-out. This assumption obviated the need for curve fitting and prevented the dose from being underestimated in organs with prolonged retention times.

Despite these conservative assumptions, the findings suggest that TISCH can be used safely in clinical investigations of the D1 dopamine receptor. The amount of activity that can be given will be limited by the dose to the colon. Federal guidelines for research in human subjects who do not directly benefit from the investigation will permit 7.5 mCi to be administered during each study. This will make it feasible to image the D1 DA receptor in patients with neuropsychiatric disorders before and after treatment.

ACKNOWLEDGMENTS

This work was supported by NIH grant NS-24538 and NIMH grant MH-43880. Special thanks go out to Medi-Physics for providing the funding to conduct the toxicology studies.

REFERENCES

1. Alexander GE, Crutcher MD, DeLong MR. Basal ganglia-thalamocortical circuits: parallel substrates for motor, oculomotor, "prefrontal" and "limbic" function. In: Uylings HBM, Van Edin CG, De Bruin JPC, Corner MA, Feenstra MGP, eds. *Progress in brain research, volume 85*. New York: Elsevier Science Publishers; 1990:119-146.
2. Waddington JL, O'Boyle KM. Drugs acting on brain dopamine receptors: a conceptual reevaluation five years after the first selective D-1 antagonist. *Pharmacol Ther* 1989;43:1-52.
3. Davis KL, Kahn RS, Ko G, Davidson M. Dopamine in schizophrenia: a review and reconceptualization. *Am J Psychiatry* 1991;148:1474-1481.
4. Davidson MD, Harvey PD, Bergman RL, et al. Effects of the D-1 antagonist SKF-38393 combined with haloperidol in schizophrenic patients. *Arch Gen Psychiatry* 1990;47:190-191.
5. Carlsson A. The current status of the dopamine hypothesis in schizophrenia. *Neuropsychopharmacol* 1988;1:179-186.
6. Pycok CJ, Kerwin RW, Carter CJ. Effects of lesions of cortical dopamine terminals on subcortical dopamine receptors in rats. *Nature* 1980;286:74-76.
7. Haroutunian V, Knott P, Davis KL. Effects of mesocortical dopaminergic lesions upon subcortical dopaminergic function. *Psychopharmacol Bull* 1988;24:341-344.
8. Hyttel J. SCH 23390: the first selective dopamine D1 antagonist. *Eur J Pharmacol* 1983;91:153-154.
9. Suhara T, Fukuda H, Inoue O, et al. Age-related changes in human D1 dopamine receptors measured by positron emission tomography. *Psychopharmacology* 1991;103:41-45.
10. Sedvall G, Farde L, Barnett A, Hall H, Halldin C. C-11 SCH 39166, a selective ligand for visualization of dopamine-D1 receptor binding in the monkey brain using PET. *Psychopharmacol* 1991;103:150-153.
11. Chumpradit S, Kung M-P, Billings JJ, Kung HK. Synthesis and resolution of (+)-7-chloro-8-hydroxy-1-(3'-iodophenyl) 3-methyl-2,3,4,5-tetrahydro-1H-3-benzazepine (TISCH): a high affinity and selective iodinated ligand for CNS D1 dopamine receptor. *J Med Chem* 1991;34:877-883.
12. Kung HF, Billings JJ, Guo Y-Z, Blau M, Ackerhalt RA. Preparation and bio-distribution of ¹²⁵I-BZP: a potential CNS D-1 dopamine receptor imaging agent. *Nucl Med Biol* 1988;15:187-193.
13. Chumpradit S, Kung M-P, Kung HF. R-(+)-7-chloro-8-hydroxy-1-(3'-[1-125]iodophenyl)-3-methyl-2,3,4,5-tetrahydro-1-H-3-benzazepine: a potential CNS D-1 dopamine receptor agent. *J Med Chem* 1989;32:1431-1435.
14. Kung M-P, Billings JJ, Alavi A, Kung HF. Effects of amphetamine and cocaine on uptake of D1 and D2 dopamine ligands in rat brain [Abstract]. *J Nucl Med* 1990;31:809.
15. Billings JB, Kung M-P, Chumpradit S, Mozley PD, Alavi A, Kung HF. In vivo characterization of [¹²⁵I] TISCH: a high affinity and selective imaging agent for the CNS D1 dopamine receptor. *J Neurochem* 1991;58:227-236.
16. Sorenson JA. Methods for quantitating radioactivity in vivo by external counting measurements. PhD Thesis (U of Wisconsin, Madison, WI) 1971.
17. Budinger TF. Progress in atomic medicine. In: Lawrence JA, ed. *Recent advances in nuclear medicine, volume 4*. New York: Grune and Stratton; 1974:41.
18. Jones JP, Brill AB, Johnson RE. The validity of an equivalent point source assumption used in quantitative scanning. *Phys Med Biol* 1975;20:455-464.
19. Thomas SR, Maxon HR. In vivo quantitation of lesion radioactivity using external counting methods. *Med Phys* 1976;3:253-255.
20. ICRP. Radiation dose to patients from radiopharmaceuticals. *ICRP publication 53, 1st edition*. Oxford: Pergamon; 1988:17-19.
21. ICRP. Limits for intake of radionuclides by workers. *ICRP Publication 30, part 1*. Oxford: Pergamon; 1979:30-34.
22. ICRP. Task group report on reference man. *ICRP Publication 23*. Oxford: Pergamon; 1975.
23. Synder WS, Ford MR. "S" absorbed dose per unit cumulated activity for selected radionuclide and organs. In: *MIRD pamphlet 11*. New York: Society of Nuclear Medicine; 1975:5-10, 172-173.
24. Sorenson AS, Phelps ME. *Physics in nuclear medicine, second edition*. Philadelphia: WB Saunders; 1987:197-217.
25. Peroutka SJ, Snyder SH. Relationships of neuroleptic drug effects at brain dopamine, serotonin, α -adrenergic, and histamine receptors to clinical potency. *Am J Psychiatry* 1980;137:1518-1522.